DNA Nanostructures

Deutsche Ausgabe: DOI: 10.1002/ange.201500175
Internationale Ausgabe: DOI: 10.1002/anie.201500175

Assembly and Purification of Enzyme-Functionalized DNA Origami Structures**

*Christopher Timm and Christof M. Niemeyer**

Abstract: *The positioning of enzymes on DNA nanostructures for the study of spatial effects in interacting biomolecular assemblies requires chemically mild immobilization procedures as well as efficient means for separating unbound proteins from the assembled constructs. We herein report the exploitation of free-flow electrophoresis (FFE) for the purification of DNA origami structures decorated with biotechnologically relevant recombinant enzymes: the S-selective $NADP^+$/NADPH-dependent oxidoreductase Gre2 from S. Cerevisiae and the reductase domain of the monooxygenase P450 BM3 from B. megaterium. The enzymes were fused with orthogonal tags to facilitate site-selective immobilization. FFE purification yielded enzyme–origami constructs whose specific activity was quantitatively analyzed. All origami-tethered enzymes were significantly more active than the free enzymes, thereby suggesting a protective influence of the large, highly charged DNA nanostructure on the stability of the proteins.*

The so-called "scaffolded DNA origami" technique,[1] wherein a long single-stranded DNA (ssDNA) scaffold is folded into any desired shape by the aid of short synthetic "staple-strand" oligonucleotides, gives ready access to an unlimited variety of finite DNA nanostructures.[2,3] Since these objects possess an addressable surface area of a few thousand square nanometers with a "single-pixel" resolution of about 6 nm,[4] DNA origami structures are currently being exploited as molecular pegboards for the precise positioning of molecular and colloidal components, such as proteins, nanoparticles, and analytical probes.[4–9] The assembly of proteins on DNA nanostructures is particularly promising because these macromolecules reveal intrinsic, evolutionarily optimized functionality, such as capability for specific molecular recognition and the catalytic conversion of ligands and substrates.[10] For example, arrangements of synthetic multienzyme cascades on DNA nanostructures are currently being exploited as spatially interactive biomolecular networks.[11] In the majority of these reported studies, commercially available glucose oxidase (GOx)/horseradish peroxidase (HRP) served as the model cascade.[12–16] Additional complexes were assembled from commercial glucose-6-phosphate dehydrogenase (G6PDH)/malic dehydrogenase (MDH)[17] or from recombinant NAD(P)H:FMN oxidoreductase/luciferase[18] or cytochrome P450 BM3 porphyrin/reductase domains[19] produced by heterologous expression.

Proteins are notoriously difficult to immobilize because instable tertiary structures often result in a significant tendency for denaturation and thus loss of activity. Therefore, to enable significant coupling efficiency and the production of enzyme-decorated DNA nanostructures with appreciable catalytic activity, the installment of enzymes on DNA nanostructures requires chemically mild coupling procedures as well as the use of a stoichiometric excess of enzymes. This strategy has the drawback that remaining unbound enzymes have to be removed to avoid artifacts in the determination of the specific activity of the multienzyme–DNA construct. Although the removal of free proteins is possible by ultrafiltration or chromatography,[16,17] this approach seems to be limited to constructs obtained from stable proteins and relatively small DNA nanoscaffolds. For example, the group of Hao Yan recently demonstrated the purification of active enzyme complexes bearing DNA double-crossover and 4×4 tiles.[17] However, our own studies indicated that BM3 porphyrin/reductase domains organized on simple double-helical scaffolds were insufficiently stable to undergo purification.[19] As an alternative, the separation of DNA origami scaffolds containing GOx and HRP model enzymes by the use of Ni–NTA-based affinity tags has been described.[20] However, this method is not always applicable because many biotechnologically relevant enzymes bear hexahistidine or other affinity tags themselves, and these tags would interfere with affinity separation. Hence, there is a great demand for broadly applicable methods in which chemoselective coupling techniques are combined with efficient means of purification of large DNA scaffolds bearing arrangements of active enzymes.

We herein report the exploitation of free-flow electrophoresis (FFE)[21,22] for the purification of rectangular DNA origami structures decorated with biotechnologically relevant enzymes through chemo- and site-selective protein–DNA coupling methods. In particular, we used the *S*-selective $NADP^+$/NADPH-dependent oxidoreductase Gre2 from *Saccharomyces Cerevisiae*, a versatile biocatalyst for the stereoselective reduction of carbonyl compounds,[23] as well as the reductase domain BMR of the monooxygenase P450 BM3 (CYP102A1) from *Bacillus megaterium*, which has been applied for the synthesis of drug metabolites and precursors of artemisinin and paclitaxel.[24] To facilitate the site-selective

[*] C. Timm, Prof. Dr. C. M. Niemeyer
Karlsruhe Institute of Technology (KIT)
Institute for Biological Interfaces (IBG 1)
Hermann-von-Helmholtz-Platz
76344 Eggenstein-Leopoldshafen (Germany)
E-mail: niemeyer@kit.edu

[**] This research was supported by the Deutsche Forschungsgemeinschaft in the course of priority programme SPP 1623 (grant NI 399/12-1). We thank Marc Skoupi for providing entry vectors for Gre2 expression and Matthias Eing for help with the experiments and the artwork.

Supporting information for this article is available on the WWW under http://dx.doi.org/10.1002/anie.201500175.

conjugation of Gre2 and BMR with DNA origami scaffolds under mild conditions, we used a previously reported approach,[25,26] which is based on the genetic fusion of the enzymes with self-labeling protein tags, that is, the "Snap-tag",[27] the "HaloTag",[28] or the streptavidin-binding peptide (SBP) tag.[29] The encoding DNA of the two enzymes was cloned into pEXP-n9 expression plasmids to enable C-terminal fusion with the HaloTag, Snap-tag, or SBP tag. Subsequent to heterologous expression, the fusion proteins were purified to homogeneity (see Figure S1 in the Supporting Information). Benzylguanine (BG) and chlorohexane (CH) groups were incorporated as suicide ligands into DNA origami to facilitate binding of the Snap- and Halo-tagged enzymes. Detailed information and experimental protocols can be found in the Supporting Information. We also explored, for the first time, the installment of biotin–streptavidin (STV) bridges on DNA origami for the selective immobilization of SBP-tagged Gre2. Subsequent to assembly, FFE-based fractionation enabled the efficient purification of active enzyme–origami structures, as demonstrated by enzyme-specific activity assays.

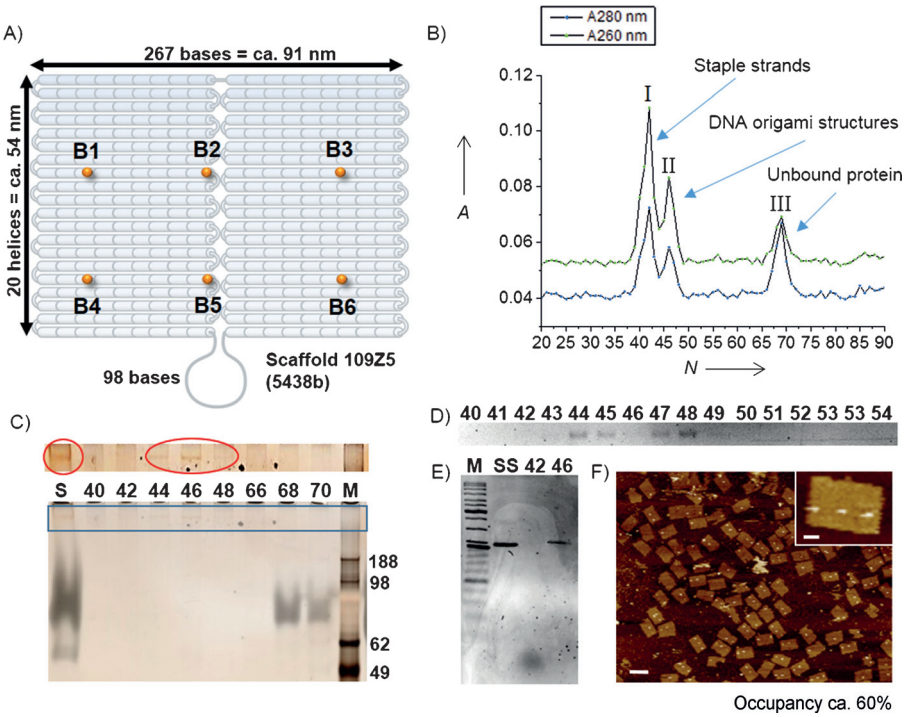

Figure 1. Streptavidin-decorated DNA origami structures. A) Origami design with six binding sites. In this experiment, only sites B4–B6 contained biotin groups. B) Absorbance measured at 260 and 280 nm of sample fractions collected after FFE separation. C) SDS-PAGE analysis (NuPAGE Novex 4–12% protein gel) of representative fractions visualized by silver staining. Samples were not boiled; therefore, the tertiary structure of STV, visible as a broad band in fractions 68 and 70 at approximately 70 kDa, was left intact. The DNA origami nanostructures showed a slight electrophoretic mobility in the upper (ca. 4%) region of the gel, as indicated by the respective bands in fractions 44–48 (red circles), visible at higher contrast in the magnified image above the gel. The crude reaction mixture and the SeeBlue Plus2 prestained standard (Invitrogen) were applied in lanes S and M, respectively. The size of marker bands is given in kDa. D) This 1% agarose gel confirms that DNA nanostructures were only present in fractions 44–48. E) This 1% agarose gel shows the presence of staple stands and folded origami structures in fractions 42 and 46, respectively, as well as the single-stranded 109Z5 template (lane SS; lane M: GeneRuler DNA Ladder Mix). F) Representative AFM image of STV-decorated DNA origami structures present in fraction 47. Scale bars are 100 and 20 nm for overview and zoom-in images, respectively.

To explore site-selective decoration and the suitability of FFE purification of large protein-decorated DNA origami structures, a DNA origami object was assembled from the single-stranded 5438 nucleotide template 109Z5.[30] The resulting DNA origami contained six binding sites located at distinguishable positions (B1–B6) on the approximately 54 × 91 nm^2 rectangular plate (Figure 1A). As an initial test, biotin groups installed in positions B4–B6 were used to capture STV molecules, applied in 80-fold molar excess to the origami (42 nM in 100 μL of TE–Mg buffer). After incubation for 120 min, the crude reaction mixture was fractionated by FFE. The FFE system consists of two parallel plates, which create a separation chamber in which the sample is transported within a thin film of the aqueous medium under laminar-flow conditions. A high-voltage electric field applied perpendicular to the laminar flow deflects charged particles, thereby enabling their separation and fractionation into wells of a microtiter plate. UV/Vis absorbance measurements of fractions with a microplate reader, followed by plotting of the measured values against the fraction number, leads to a reconstructed chromatogram in which peaks indicate separated species (Figure 1B). Gel electrophoretic analysis of fractions (Figure 1C,D) indicated the separation of staple strands, DNA origami structures, and free protein (peaks I–III in Figure 1B, respectively). AFM analysis of fraction 46 revealed the presence of intact and pure STV-decorated DNA origami structures. Statistical analysis indicated that 60% of the biotin binding sites were occupied by STV molecules. Importantly, no damaged origami structures were observed, thereby suggesting that FFE purification does not exert significant mechanical stress on the fragile protein–DNA nanostructures.

We then tested FFE for the purification of DNA origami structures decorated with recombinant enzymes (Figure 2). In a first set of experiments, DNA origami containing BG or CH groups at positions B4–B6 (Figure 1A) was treated with a 260-fold molar excess of Gre2–Snap (Figure 2A) or Gre2–Halo (Figure 2B) fusion proteins, respectively. FFE separation of the reaction mixture led to the fractionation of DNA- and protein-containing samples, as determined by electrophoresis with either DNA- or protein-specific gels and

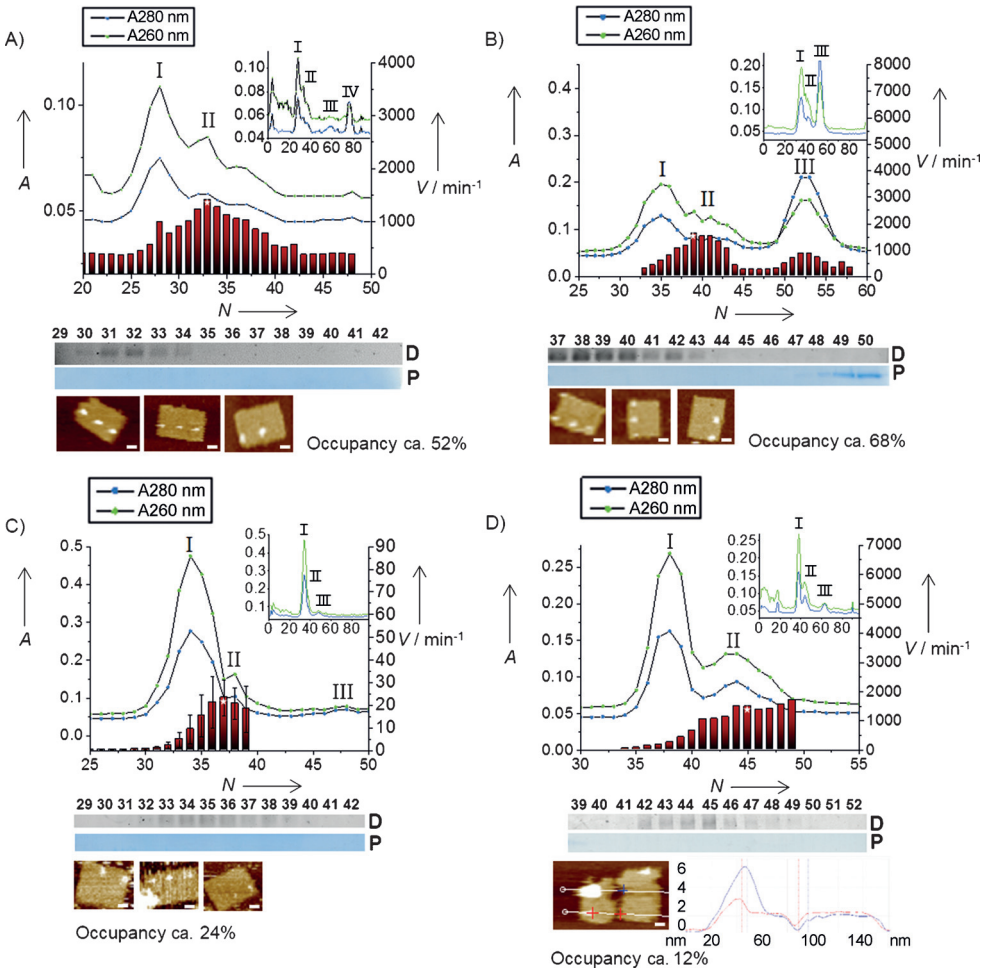

Figure 2. Purification and characterization of DNA origami scaffolds decorated with the recombinant enzymes A) Gre2–SNAP, B) Gre2–Halo, C) BMR–Halo, and D) Gre2–SBP. In each case, the absorbance of relevant FFE fractions at 260 and 280 nm is shown in the main graph, and an inset shows the absorbance for the entire set of fractions. The red bars underneath the absorbance curves indicate the specific reaction velocity determined for the individual fractions (see the Supporting Information). In each case, the fraction displaying highest activity is marked with an asterisk. The electrophoretic detection of DNA (D) and proteins (P) in the fractions is shown below each graph in the relevant portions of agarose and SDS-PAGE gels, respectively. No free protein was visible in the fractions containing origami (see also Figure S2–S4). Gel electrophoresis was carried out as described for Figure 1. Representative AFM images of enzyme-decorated DNA origami structures are shown below the images of the gels (scale bars: 20 nm). Surface occupancies were in a similar range to that previously observed for the Snap- and Halo-tag-based conjugation of enzymes onto DNA origami structures.[25] The height measurements shown at the bottom of (D) indicate bound Gre2 through elevated height (about 6 nm) as compared to that observed for STV alone (ca. 2 nm) or unmodified DNA origami structures (ca. 1 nm).

staining procedures (images labeled as D or P, respectively, in Figure 2). In particular, origami constructs were found in fractions 31–34 or 37–44, whereas unbound protein was found in fractions 51–56 or 48–57 of Snap- or Halo-fusion constructs, respectively (see Figure S2).

All fractions which contained protein were analyzed for enzymatic activity by measuring the initial reaction velocities of Gre2-catalyzed $NADP^+$ reduction to NADPH. To obtain a quantitative measure for specific activity (red bars in Figure 2), we normalized reaction velocity data against the amount of protein in the fractions. To this end, the protein concentration was determined from UV/Vis spectroscopic measurements in the case of samples containing protein only (e.g., fractions 59 and 53 in Figure 2A and B, respectively). In the case of enzyme–origami structures, amounts of Gre2–Snap (fraction 33 in Figure 2A) or Gre2–Halo (fraction 39 in Figure 2B) were calculated from the origami concentration and surface occupancy, as determined by quantitative PCR and AFM, respectively (see the Supporting Information for details). The data clearly indicate that activity was highest in samples containing the Gre2-decorated origami constructs. Similar specific activity was found for Gre2–Snap and Gre2–Halo constructs, whereas surface occupancy was slightly higher in the case of Gre2–Halo, as determined by the statistical analysis of AFM images. The latter suggested that coupling reactions were more effective for the Halo-based fusion proteins than for Snap fusions.

Similar experiments were carried out for the binding of BMR–Halo on DNA origami (Figure 2C). Gel electrophoretic analysis confirmed that fractions containing origami constructs (32–39, peak I) were indeed baseline separated from unbound BMR (fractions 44–52, peak III) upon FFE fractionation. The highest specific enzyme activity was found in fractions 36–39, as determined by the NADPH-dependent reduction of cytochrome C (CytC; see the Supporting Information). Despite the use of the same coupling protein, surface occupancy was significantly lower than that observed for Gre2–Halo (24 versus 68%). We reason that this difference is a consequence of the lower isoelectric point (pI) of BMR (pI = 5.02) as compared to Gre2 (pI = 5.86). We had previously observed that proteins with lower pI values bind less efficiently than those with higher pI values, presumably as a result of higher electrostatic repulsion between the proteins and negatively charged origami.[25]

We also tested the immobilization of SBP-tagged Gre2 through biotin–STV bridges on the DNA origami. To this end, biotin groups installed at positions B4–B6 (Figure 1A) of the

origami were exposed to STV (80 molar equivalents), and the mixture was purified by FFE and subsequently incubated with an 80-fold molar excess of the Gre2–SBP protein. Gel electrophoresis indicated that FFE fractions 42–50 contained origami constructs that were baseline-separated from unbound Gre2–SBP (fractions 60–68, peak III in Figure 2D). The Gre2 enzymatic activity found in fractions 45–50 (orange bars), together with the AFM analysis of origami structures from fraction 45, provided clear evidence that the noncovalent coupling of Gre2–SBP had occurred in the expected manner.

We then used the above-described coupling and separation techniques for the construction and characterization of an enzyme cascade containing Gre2–Snap and BMR–Halo installed on DNA origami (Figure 3). In this cascade, Gre2-catalyzed $NADP^+$ reduction yields NADPH, which is used for the BMR-catalyzed reduction of cytochrome C (Figure 3A). The origami bearing BG and CH affinity ligands was treated with a mixture containing a 120-fold molar excess of each of the two orthogonally tagged enzymes. Samples obtained upon FFE fractionation were analyzed by absorbance measurements (Figure 3B), electrophoresis (Figure 3C,D), AFM (Figure 3E), and enzyme-activity assays (Figure 4A). Similarly to the previous examples, electrophoretic analyses confirmed the baseline separation of origami constructs (fractions 33–40) and unbound proteins (fractions 41–48) upon FFE fractionation. Analysis of the enzymatic activity indicated that fractions 33–39 contained the origami–Gre2/BMR cascade systems. Owing to positional encoding and the larger size of BMR as compared to Gre2 (101.6 and 60.8 kDA, respectively), unambiguous identification of the two proteins was possible by AFM analysis of the purified constructs (Figure 3E). Statistical evaluation showed surface occupancies of 49 and 63% for Gre2–Snap and BMR–Halo, respectively. We speculate that the higher occupancy of

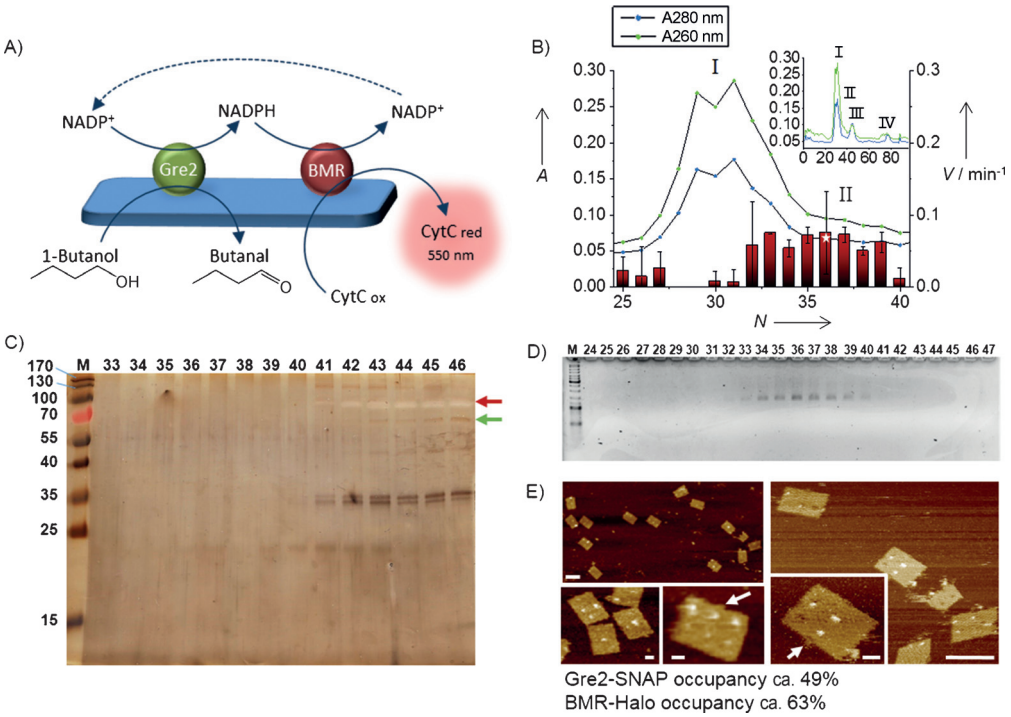

Figure 3. Enzyme-cascade complex of Gre2–Snap and BMR–Halo on DNA origami. A) Schematic drawing of the enzyme cascade and the activity assay. B) Absorbance of relevant FFE fractions at 260 and 280 nm (the inset shows the absorbance of the entire set of fractions at these wavelengths). The red bars indicate the specific reaction velocity determined for the individual fractions (see Table S5 in the Supporting Information). C) Silver-stained 16% SDS-PAGE gel indicating the presence of unbound protein in fractions 41–46. Marker bands are given in kDa; bands of Gre2–Snap and BMR–Halo are indicated by a green and a red arrow, respectively; the bands at a molecular weight of approximately 35 kDa presumably stem from degradation products of an enzyme. D) Agarose-gel analysis indicating the presence of origami in fractions 33–40. Lane M: GeneRuler DNA Ladder Mix. E) AFM images of immobilized Gre2–Snap and BMR–Halo bound to positions B1–B3 and B4–B6, respectively, on DNA origami. The white arrows mark the loop of the DNA origami structures. Scale bars are 100 and 20 nm for overview and zoom-in images, respectively.

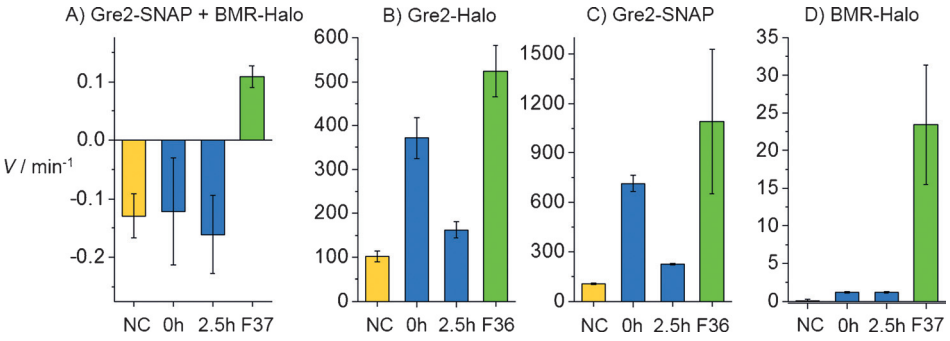

Figure 4. Comparison of reaction velocities determined for origami-tethered enzymes (green bars) as well as free enzymes (blue bars), freshly prepared (0 h) or incubated for 2.5 h. For NC = negative control, the sample contained buffer only. A) Gre2–SNAP/BMR–Halo cascade; B) Gre2–Halo; C) Gre2–SNAP; D) BMR–Halo. The negative values observed in (A) for samples containing free enzymes as well as for the negative control stem from the decrease in CytC absorbance over time owing to the autooxidation of CytC in air, a phenomenon typically observed in the CytC reduction assay[33] (see also original data in Figure S9).

BMR–Halo than in the single-enzyme-binding experiments (Figure 2C) could be due to favorable protein–protein interactions in this cascade arrangement.

To assess the enzymatic activity of the purified origami-scaffolded Gre2/BMR cascade we determined specific activities, for which the observed initial reaction velocity was normalized in each case against the amount of enzymes present in the sample (see the Supporting Information). This approach enabled direct comparison of the activity of origami-tethered enzymes with that of controls prepared from identical amounts and concentrations of free enzymes (Figure 4). The activity of the controls was either measured immediately after preparation or after incubation for 2.5 h, the typical time period needed for coupling and FFE separation of the enzyme–origami constructs (bars labeled as 0 or 2.5 h, respectively, in the histograms in Figure 4). Strikingly, no activity was measured in the controls containing free Gre2–Snap and BMR–Halo enzymes, whereas significant activity was clearly observable in the case of the origami-scaffolded cascade (Figure 4A; see also Figure S9). Indeed, this increased activity was expected from previous reports and can be explained by spatial proximity effects enabling a faster diffusive transport of the intermediate (in this case NADPH) between cascaded enzymes.[11–18] However, similar controls carried out with the two individual enzymes also revealed a significantly increased activity of the origami-tethered enzymes as compared to free enzymes in solution (Figure 4B–D). Taking into account that all controls lose significant activity upon incubation (compare the data recorded at 0 and 2.5 h), we speculate that a plausible explanation for this phenomenon is that the large, highly charged DNA nanostructure protects the enzyme against denaturation, for example, upon physisorption on the surface of the reaction vessel. Notably, the protective influence of DNA nanostructures needs to be taken into account when DNA-cascaded enzymes are studied on a quantitative level.

In conclusion, we herein demonstrated, for the first time, that free-flow electrophoresis (FFE) is very well suited for the purification of enzyme-decorated DNA origami structures. Alternative methods, such as agarose-gel electrophoresis, HPLC, ultrafiltration, dialysis, or rate-zonal centrifugation,[31] require relatively long processing times of at least 1–3 h and/or exert chemical and mechanical stress on the large and fragile protein–DNA nanostructures. In contrast, FFE is fast (ca. 10–15 min), proceeds under mild physicochemical conditions, and led to pure and active enzyme–origami constructs that were isolated in good yields of typically 50–70%. Moreover, FFE offers numerous approaches for the further improvement of separation efficiency through optimization of the pH value, ion strength, and viscosity of buffers, the use of alternative separation techniques, such as zone electrophoresis and isoelectric focusing, or miniaturization of the system.[22,32] Hence, specific optimization might even enable the separation of distinctive protein–DNA nanostructure species in the future. In the initial exploitation presented herein, the mildness and velocity of FFE enabled us to quantify the specific activity of enzyme–origami constructs that were not biased by free, unbound proteins. In all cases, we observed that the activity of enzymes coupled to origami structures was greater than that of the free enzymes. These findings suggest that the DNA nanostructure has a general protective influence on the stability of tethered proteins. Moreover, our study emphasizes the practical relevance of chemoselective coupling techniques for the site-specific arrangement of biotechnologically relevant, recombinant enzymes through genetically fused tags. In addition to the use of Snap- and Halo-tagged proteins,[25] the utility of the SBP tag extends the toolbox for this approach. We believe that the methods described herein provide a sound basis for further quantitative assessment of arrangements of synthetic multienzyme cascades on DNA nanostructures and other spatially interactive biomolecular networks.[11]

Keywords: DNA nanostructures · enzymes · free-flow electrophoresis · purification methods · self-assembly

How to cite: *Angew. Chem. Int. Ed.* **2015**, *54*, 6745–6750
Angew. Chem. **2015**, *127*, 6849–6854

[1] P. W. Rothemund, *Nature* **2006**, *440*, 297.
[2] J. Nangreave, D. Han, Y. Liu, H. Yan, *Curr. Opin. Chem. Biol.* **2010**, *14*, 608.
[3] W. M. Shih, C. Lin, *Curr. Opin. Struct. Biol.* **2010**, *20*, 276.
[4] B. Saccà, C. M. Niemeyer, *Angew. Chem. Int. Ed.* **2012**, *51*, 58; *Angew. Chem.* **2012**, *124*, 60.
[5] A. M. Hung, H. Noh, J. N. Cha, *Nanoscale* **2010**, *2*, 2530.
[6] T. Tørring, N. V. Voigt, J. Nangreave, H. Yan, K. V. Gothelf, *Chem. Soc. Rev.* **2011**, *40*, 5636.
[7] F. C. Simmel, *Curr. Opin. Biotechnol.* **2012**, *23*, 516.
[8] A. Rajendran, M. Endo, H. Sugiyama, *Angew. Chem. Int. Ed.* **2012**, *51*, 874; *Angew. Chem.* **2012**, *124*, 898.
[9] Q. Liu, C. Song, Z. G. Wang, N. Li, B. Ding, *Methods* **2014**, *67*, 205.
[10] C. M. Niemeyer, *Angew. Chem. Int. Ed.* **2010**, *49*, 1200; *Angew. Chem.* **2010**, *122*, 1220.
[11] J. Fu, M. Liu, Y. Liu, H. Yan, *Acc. Chem. Res.* **2012**, *45*, 1215.
[12] J. Müller, C. M. Niemeyer, *Biochem. Biophys. Res. Commun.* **2008**, *377*, 62.
[13] O. I. Wilner, S. Shimron, Y. Weizmann, Z. G. Wang, I. Willner, *Nano Lett.* **2009**, *9*, 2040.
[14] O. I. Wilner, Y. Weizmann, R. Gill, O. Lioubashevski, R. Freeman, I. Willner, *Nat. Nanotechnol.* **2009**, *4*, 249.
[15] J. Fu, M. Liu, Y. Liu, N. W. Woodbury, H. Yan, *J. Am. Chem. Soc.* **2012**, *134*, 5516.
[16] Y. Fu, D. Zeng, J. Chao, Y. Jin, Z. Zhang, H. Liu, D. Li, H. Ma, Q. Huang, K. V. Gothelf, C. Fan, *J. Am. Chem. Soc.* **2013**, *135*, 696.
[17] J. Fu, Y. R. Yang, A. Johnson-Buck, M. Liu, Y. Liu, N. G. Walter, N. W. Woodbury, H. Yan, *Nat. Nanotechnol.* **2014**, *9*, 531.
[18] C. M. Niemeyer, J. Koehler, C. Wuerdemann, *ChemBioChem* **2002**, *3*, 242.
[19] M. Erkelenz, C. H. Kuo, C. M. Niemeyer, *J. Am. Chem. Soc.* **2011**, *133*, 16111.
[20] K. Numajiri, T. Yamazaki, M. Kimura, A. Kuzuya, M. Komiyama, *J. Am. Chem. Soc.* **2010**, *132*, 9937.
[21] L. Křivánková, P. Boček, *Electrophoresis* **1998**, *19*, 1064.
[22] R. Wildgruber, G. Weber, P. Wise, D. Grimm, J. Bauer, *Proteomics* **2014**, *14*, 629.
[23] M. Müller, M. Katzberg, M. Bertau, W. Hummel, *Org. Biomol. Chem.* **2010**, *8*, 1540.
[24] S. T. Jung, R. Lauchli, F. H. Arnold, *Curr. Opin. Biotechnol.* **2011**, *22*, 809.
[25] B. Saccà, R. Meyer, M. Erkelenz, K. Kiko, A. Arndt, H. Schroeder, K. S. Rabe, C. M. Niemeyer, *Angew. Chem. Int. Ed.* **2010**, *49*, 9378; *Angew. Chem.* **2010**, *122*, 9568.

[26] R. Meyer, C. M. Niemeyer, *Small* **2011**, *7*, 3211.
[27] A. Keppler, S. Gendreizig, T. Gronemeyer, H. Pick, H. Vogel, K. Johnsson, *Nat. Biotechnol.* **2003**, *21*, 86.
[28] G. V. Los, K. Wood, *Methods Mol. Biol.* **2007**, *356*, 195.
[29] A. D. Keefe, D. S. Wilson, B. Seelig, J. W. Szostak, *Protein Expression Purif.* **2001**, *23*, 440.
[30] M. Erkelenz, D. M. Bauer, R. Meyer, C. Gatsogiannis, S. Raunser, B. Sacca, C. M. Niemeyer, *Small* **2014**, *10*, 73.
[31] C. Lin, S. D. Perrault, M. Kwak, F. Graf, W. M. Shih, *Nucleic Acids Res.* **2013**, *41*, e40.
[32] D. Kohlheyer, J. C. Eijkel, A. van den Berg, R. B. Schasfoort, *Electrophoresis* **2008**, *29*, 977.
[33] Y. R. Chen, L. J. Deterding, B. E. Sturgeon, K. B. Tomer, R. P. Mason, *J. Biol. Chem.* **2002**, *277*, 29781.

Received: January 8, 2015
Revised: March 7, 2015
Published online: April 27, 2015

